ICES Journal of Marine Science

ICES Journal of Marine Science (2016), doi:10.1093/icesjms/fsw211

Method to observe large scale behavioural waves propagating through fish schools using 4D sonar

Nils Olav Handegard[1,*], Arne Johannes Holmin[1] and Guillaume Rieucau[1,2]

[1]*Institute of Marine Research, PO Box 1870 Nordnes, Bergen 5817, Norway*
[2]*Florida International University, Biscayne Bay Campus, Marine Sciences Building, North Miami, FL, USA*

**Corresponding author: tel: +47 95854057; fax: +47 55238531; email: nilsolav@imr.no*

Handegard, N. O., Holmin, A. J. and Rieucau, G. Method to observe large scale behavioural waves propagating through fish schools using 4D sonar. – ICES Journal of Marine Science, doi:10.1093/icesjms/fsw211.

Received 25 April 2016; revised 31 August 2016; accepted 28 September 2016.

How animals interact collectively in groups is of interest for both ecologists and engineers, both from a mechanistic and functional point of view. A property of some large animal groups, regardless of their size, is their ability to perform highly coordinated anti-predatory reactions that can progress through entire groups. We developed a method using a true 3D sonar to quantify these behavioural waves in free-ranging fish schools, utilizing that rapid changes is backscattering strength is caused by changes in fish orientation rather than changes in density. Both simulated and real data were used for evaluation of the method. The method reliably estimated the speed of a simulated turning wave propagating through the school, and tests on real data gave similar wave speeds as observed in smaller scale experiments. In cases where the schools were highly irregular and dynamic, the results were less reliable. These cases were identified by high sensitivity to the classification parameters. Until now, the existing methodology has been restricted to small scale laboratory experiments or qualitative observations. Our approach provides a tool to validate the generalizations that are usually extrapolated from small scale tank studies, and we discuss its potential use.

Keywords: collective behaviour, predator avoidance, schooling behaviour, sonar, turning wave.

Introduction

Fish schooling is a remarkable example of collective behaviour, and the phenomenon has been a field of scientific focus since Parr's seminal paper almost 100 years ago (Parr, 1927). How fish organize and maintain schools from a mechanistic basis to a functional role in predator avoidance and survival is still an active field of research (Hofmann *et al.*, 2014). It has been shown how animal groups can move in unison (Buhl *et al.*, 2006), self-organise and form complex dynamic patterns (Ballerini *et al.*, 2008; Cavagna *et al.*, 2010), make collective decisions (Couzin *et al.*, 2005), increase their swimming efficiency (Hemelrijk *et al.*, 2015), or collectively sense, and follow environmental gradients (Berdahl *et al.*, 2013).

A question of particular interest is how individuals within schools or flocks transmit and receive information between members of the group. When looking at the patterns from schools and flocks, the level of synchrony is truly mesmerising. When one fish reacts, either spontaneous or to a threat, the reaction spreads through the school making the other individuals aware. These behavioural waves, or "waves of agitation" (Radakov, 1973), moves faster than the swimming speed of fish and allows the signal to be transmitted efficiently through the school. This signalling do also occur in insects and was coined the Trafalgar effect (Treherne and Foster, 1981) referring to how the English ships communicated using signal flags during the battle of Trafalgar.

Modelling the interactions between individuals and evaluating the emergent properties have been a common strategy when studying this phenomenon (Lopez *et al.*, 2012). The models are commonly inspired by physics and the interactions between individuals are usually modelled as physical "forces" where the forces represent one individuals' influence on another. An early implementation of an individual based computer model was made in 1987 (Reynolds, 1987), where the different "forces" were implemented as attraction, repulsion and alignment and the reaction to

a predator was modelled as a strong repulsive force. Similar approaches have been used for schooling fish (Huth and Wissel, 1992) and schools attacked by predators (Vabø and Nøttestad, 1997). These classes of models usually assumes homogeneity in how the different agents influence each other, either by assuming a sphere of influence or a fixed number of influencing agents (Ballerini *et al.*, 2008), and data from video analysis and automated tracking algorithms have been used estimate the zones of influence (Herbert-Read *et al.*, 2011; Katz *et al.*, 2011). More recently, data on the individuals that influence the group have become available (Nagy *et al.*, 2010; Rosenthal *et al.*, 2015), and there are more heterogeneity than assumed in the earlier models. These recent advances have been made possible by developing novel observation methodology, both for tank experiments and in situ observations, and it is likely that improved observation methods will further support this development.

For aquatic systems, the principal challenge to using optics is visibility, restricting it to laboratory studies (Katz *et al.*, 2011), smaller scale mesocosm studies (Marras *et al.*, 2012) or tracking of near surface schools. However, due to favourable propagation properties in water, active acoustic systems have been successfully applied to observe marine life (Benoit-Bird and Lawson, 2016), from vertical aggregation patterns in spawning cod (*Gadus morhua*) using echo sounders (Sund, 1935), school structure and distribution using fisheries sonar (Fréon *et al.*, 1992; Misund, 1993; Pitcher *et al.*, 1996), fine scale predator prey interactions and dynamic schooling behaviour using acoustic imaging (Axelsen *et al.*, 2001; Handegard *et al.*, 2012; Rieucau *et al.*, 2015), structure and information transfer in marine schools (Gerlotto *et al.*, 2006), to large-scale compressional forming waves of oceanic shoals (Makris *et al.*, 2009).

Acoustic reflection from a fish varies with the frequency of the incoming sound pulse but is also highly dependent on angle of ensonification, where a weak acoustic reflection is generated when ensonified head or tail on as opposed to side aspect (Lilja *et al.*, 2004; Pedersen *et al.*, 2009; Holmin *et al.*, 2012). This is what caused the behavioural waves to be observable in (Gerlotto *et al.*, 2006), where they visually tracked this wave using a 3D sonar (two spatial dimensions and time). Changes in fish volumetric density will also cause changes in acoustic backscatter (Jagannathan *et al.*, 2010; Bertsatos and Makris, 2011), but this occurs on a different time scale and is bounded by the swimming speed of the fish. Changes that occur on shorter temporal scales than those that can be explained by fish density can thus be attributed to changes in orientation of the fish. This can be exploited to estimate information transfer in wild fish schools.

Currently there is no methodology beyond simple visual tracking that allows the estimation of these behavioural waves in free-ranging fish schools in the open ocean in time and 3D space. The objective of this paper is to present a methodology capable of extracting the large scale behavioural waves seen in wild fish school using a 4D multi beam sonar (Ona *et al.*, 2009), where three spatial dimensions are ensonified at each time step, and the waves are estimated in 3D and time.

Materials and methods

The concept

The concept utilizes the fact that the ensonification angle of the fish relative to the sonar changes when a wave of turning progresses through the school. This causes the backscatter to change rapidly, and when the change in backscatter occurs on a temporal scale that is shorter than changes due to fish movement, the change can be attributed to a turning event, as opposed to density changes.

Properties of the sonar

The sonar used in this study was the Simrad MS70 multibeam sonar (Kongsberg Maritime AS, Horten, Norway), but the method is general and can be applied to any sonar system that is sensitive to backscatter changes due to orientation changes. The MS70 has 500 individual beams set up in 20 horizontal fans. Each fan operates at a different frequency and is comprised of 25 individual beams spanning 60° horizontally. The 20 fans are uniformly spaced to cover 45° vertically, where the lowest fan operates at 112 kHz and is directed 45° downward and the uppermost fan operates at 75 kHz and is directed parallel to the water surface (Ona *et al.*, 2009; Holmin *et al.*, 2012). The pulse repetition interval in this study was on average 1.7 s.

The sonar output is calibrated volume backscattering strength $s_v(ijt)$ (Maclennan *et al.*, 2002) resolved in range interval i and time step t for each sonar beam j. Each s_v value depends on the number of fish, the mean fish orientation, and the acoustical properties of the fish within a voxel volume of $V(ijt)$. The voxels are disjoint 3D volume elements defined by a 3D spherical grid comprised of range from the sonar and azimuth and elevation angle defined by the directions of the beams. The extent of the voxels along the beams is constant (0.38 m, given by the acoustical sampling interval duration), whereas the extent across the beams increases linearly by range (~10 m at 250 m range), resulting in higher resolution along than across beams at longer ranges.

Due to the elongation of the voxels of the sonar, classical interpolation of the midpoints of the voxels into a cubic Cartesian grid is not trivial, with a large variation in the number of voxel midpoints located in each grid cell. Instead, we took a different approach where the acoustic energy is distributed throughout each voxel of the sonar and subsequently accumulated in each voxel of a georeferenced cubic Cartesian grid. The grid is represented by the three spatial dimensions (x, y, z) and time, with indices k, l, m, and t, respectively (c.f. SI for details). This method preserves the effect of elongated voxels, but includes a random component that introduces some variability in the gridded backscattering strength $s_v(klmt)$. A grid spacing of $\Delta d = 5m$ was used in all cases.

Filtering, segmentation, and "school volume"

A smoothing spline is used to filter the data. The filtering is applied along the three spatial dimensions using a smoothing procedure for uniformly sampled datasets (Garcia, 2010). The filter is applied in space for each time step separately and the filtered values are denoted s'_v. The algorithm is robust towards outliers. The degree of smoothing needs to be fairly high to pick up the larger scale patterns, and we used a manually set smoothing parameter p as input to the smoothing spline algorithm. The resulting data is a smooth version of the echo energies within each voxel.

The next step is to identify the voxels with strong backscatter to those with no fish or low backscatter due to the fish orientating away from the transducer. To do this the smoothed s'v values are thresholded:

$$\mathrm{B}(klmt) = \begin{cases} 0 \text{ if } s'_v < h \\ 1 \text{ if } s'_v \geq h \end{cases}, \quad (1)$$

where h is determined by minimizing the intraclass variance of the set of voxels for classes defined by B (Otsu, 1979); using the Matlab function *graythresh*. The value h is calculated for each ping in segments of N pings, and the median h over the N pings is used in the subsequent analysis. The value of N can be interpreted as the number of pings we track the surface of one particular echo energy level, see edge tracking below. In our test cases N is equal to the duration of the data sets.

The volume defined by the surface of constant h (where $B = 1$) is determined by summing B over the three spatial dimensions and multiplying by $(\Delta d)^3$. When the volume increases or decreases on a short time scale for a fixed h, while assuming stationary density, an increasing number of fish are oriented broadside or head/tail on to the sonar, respectively. This is an indicator of strong internal dynamics in the school and can be used as a global and robust metric of internal fluctuations in a school.

To detect and calculate the speed of a behavioural wave progressing through the school, we first connect the voxels that are above the threshold ($B = 1$) using a full 4D connectivity matrix structure, i.e. any adjacent (in terms of both surface and corners) voxels in any dimension (including time) are connected to one cluster of connected voxels (using the Matlab function *bwconncomp*). The sub sets of $B = 1$ that form these connected clusters are denoted B_i where i denotes the cluster number. If the voxels are connected in time, they belong to the same school and any voids that appear on short time scales within that cluster are attributed to orientation changes. If two separate clusters/schools are in the field of view of the sonar, they are treated as separately in the following analysis. This approach avoids overestimation of the waves in case one school disappears entirely and the boundary of the lost school is associated with that of the remaining school.

If two separate clusters in a single time step are connected at later time steps, they belong to the same cluster. This may cause overestimation of the track velocities if one part of the cluster disappears and gets tracked to the other part (see explanation of method below). For large schools with several sub clusters this will cause challenges, but in those cases it is also difficult to reliably associate changes in backscatter to a propagating wave although internal structure may be highly dynamic. For these cases the change in volume may be used a measure of the internal fluctuations.

When a propagating turning wave progresses through the school, the change will be visible as a moving surface of constant h. An estimate of the wave is found by estimating the velocity of the surface (Figure 1). To do so, we first detect the voxels that are on the surface of the connected structure B_i. The surface voxels are defined as those voxels that have less than six adjacent neighbours. Here adjacent means voxels that share a surface as opposed to the connectivity algorithm where it could also share a corner of a voxel. Voxels intersecting with the edges of the sonar volume is excluded from the set of surface voxels to avoid tracking the edge of the sonar as a turning wave, e.g. if the vessel is turning. This results in a set of surface voxels for the edge tracking for each connected structure B_i.

To track the surface, we start at the central position of each surface voxel at time step t. The surface voxel j belonging to each sub structure B_i for time step t is denoted $x_{it}(j, 0)$, where "0"

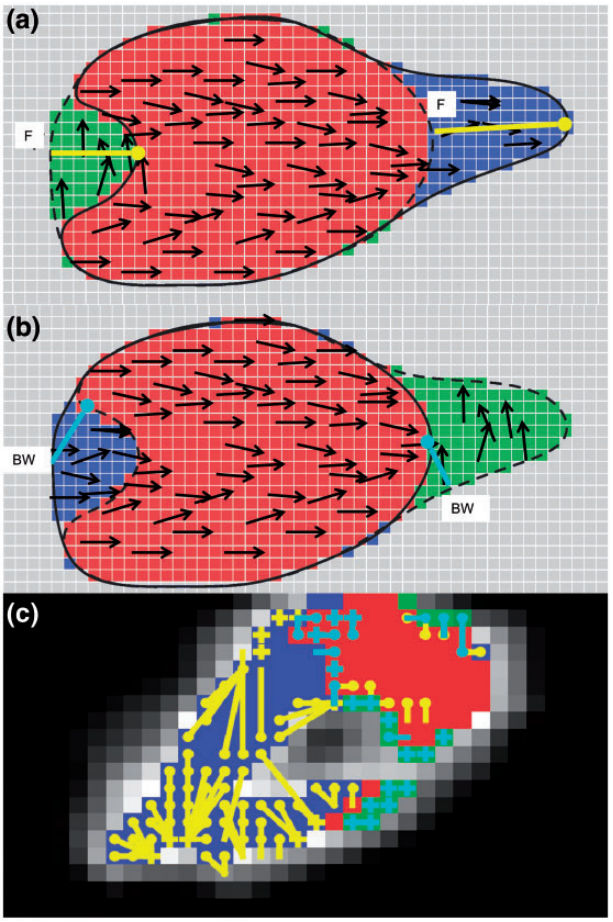

Figure 1. A conceptual school at two consecutive pings (a,b) and a real example (c) to illustrate the method. The fish alignments are indicated by the arrows and change from (A) to (B), and the resulting surface formed by the segmented volume B_i for each time step is depicted by the solid black line. The broken lines are the segmentation volume in the following (A) or previous (B) time step, respectively, to illustrate how the forward (F) and backward (BW) tracking work. In (A), the green and blue pixels are the gained and lost pixels between (A) and (B), respectively, and the yellow lines show two F tracks where the yellow dot is the starting point. In (B), the green and blue pixels are the gained and lost pixels between (B) and (A), respectively, when tracking BW (opposite of A). The cyan arrows show two (BW) tracks for illustration. In this particular example, the forward tracks (yellow) works as anticipated while the backward tracks (cyan) underestimate the change of surface. (C) Real data example. Blue pixels are pixels that are lost in the next time step, green pixels are gained the next time step and red pixels are within the volume in both time steps. The yellow and cyan lines are the F and B tracks, respectively, where the dots indicate the starting position, similar to (A) and (B). Note that the ending position does not have to be in the same plane, and that is the reason why the tracks do not necessarily end in a red or cyan pixel.

indicates that this is the initial positions for the surface tracks. The tracks are then formed by finding the *nearest* surface voxel in the subsequent time step, with position $x_{it}(j, 1)$, where "1" denotes that we have moved one time step ahead. This is repeated for M time steps resulting in a track of surface voxels over $M + 1$ time steps. The parameter M denotes how many time steps the surface is tracked before estimating a velocity. $M > 1$ is used to

avoid random back and forth fluctuations to be detected as a propagating wave, whereas using $M = 1$ might be used if the waves are fast compared with the ping rate (but this is vulnerable to noise). If M is too large the method will not discriminate between density changes and orientation changes. This results in a set of surface trajectories for each surface voxel in time step t, and the mean velocity is representative for time step $t + \frac{1}{2}M$ (half time steps implies average time of consecutive time steps).

The tracking of the surface works well if the shape of the boundary is convex or close to convex (Figure 1A and C), but this is not always the case. If the fish turn such that the boundary moves away from the centre of the school (Figure 1A, left part), the starting point of the wave will not be clearly defined, and the concave shape may close causing overestimation of the speed. These shapes are typically sensitive to the thresholding parameter, and can be detected by checking the sensitivity to the thresholding parameter h. In other cases the forward tracking will underestimate the wave since the nearest surface voxel may be in a different direction than the wave propagates. This is dealt with by running the algorithm both back and forth over the M pings, resulting in two sets of surface tracks, from both forward and backward tracking (Compare Figure 1A and B).

When all the trajectories are established for the range of M pings, the mean velocity for each trajectory is calculated, and the highest speed among the forward and backward trajectories is selected as the wave speed for that time interval.

The next time step $(t + 1)$ is then selected and the procedure is repeated.

Results

To assess the efficacy of the method, we used both a simulation experiment (Case I) and tests on real data (Cases II and III). The simulation experiment was designed to evaluate whether the method works on a simulated information transfer wave progressing through a school, and the real test cases were picked to illustrate different aspects of the method's performance.

Simulation experiment (Case I)

The advantage of a simulation experiment is that it allows for control of the underlying mechanism that generates the data. To do this, we simulated a school of individual herring with initial orientation perpendicular to the sonar beam (Figure 2A). The fish were randomly distributed in an ellipsoid with semi axes 50, 35, and 10 m in the x, y, and z direction of the global coordinate system, centred at 150 m depth. An autoregressive component was added to the positions of each fish, inducing a desired polarization of 16.9°, i.e. the mean angle deviation between orientation of the individuals and the school (Parrish *et al.*, 2002). We did not include any interaction between the fish, but any individual based model taking such interactions into account could have been used to predict the resultant scattering. After five initial time steps, a turning wave started at $x = -50$ m progressing at a speed of 15 m/s across the school towards positive x (see Figure 2B). The fish inside the wave were turned by 60° away from the vessel. After four time steps the wave stopped, followed by five time steps with stationary fish orientation.

The corresponding acoustic signal was generated using a simulation framework for acoustic data including noise (Holmin *et al.*, 2016), where the contributions of the individual fish to the total echo was summed and where the interference scattering was taken into account. The individual herring were represented acoustically by prolate spheroids (Tang *et al.*, 2009) with an aspect ratio of 5 (corresponding to oblong fish, used by Holmin *et al.*, 2012, 2016), resulting in highly directional backscatter, as observed for real herring (Pedersen *et al.*, 2009). Extinction, which is the weakening of the signal due to high fish density (Zhao and Ona, 2003), was not taken into account in the version of the model used in this article. The resulting backscattering caused the school to "disappear" starting from $x = -50$ at time step 5 as the wave progressed through the school (Figure 2B).

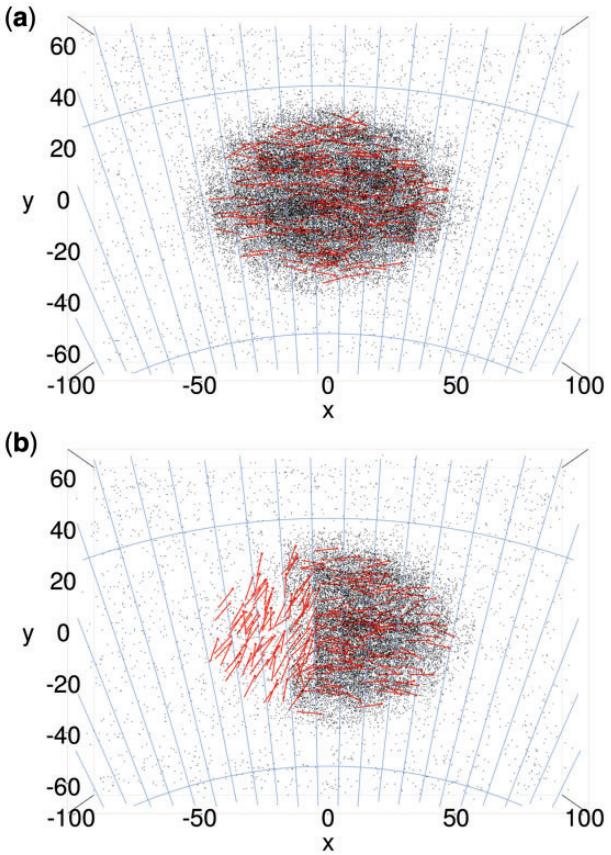

Figure 2. Example of simulated data at time step 1 (a) and time step 8 (b). The red lines are the direction of the fish and the density of the black dots is proportional to the estimated backscatter. The effect of fish orientation is clearly seen as the turning wave progresses through the school (B).

The methodology was applied to the test data set to assess whether we could reliably estimate the wave speed of 15 ms^{-1} from the simulated data. The first step was to convert the data to Cartesian coordinates (see SI), smooth the data, and segment the high backscatter parts of the school used in the edge tracking algorithm. A smoothing of $p = 0.2$ was used and the threshold used for the segmentation was estimated by Otsu's algorithm as described in the method section. The resulting segmentation is shown Supplementary Figure S1. Since these values may affect the performance of the algorithm, the sensitivity to these parameters was assessed by generating the results for a range of the parameters, similar to a sensitivity analysis. The smoothing parameter was set to $p \in \{0.1\ 0.2\ 0.3\}$, whereas the threshold estimated by Otsu's method was multiplied by a factor of $k \in \{0.8\ 1.0\ 1.2\}$.

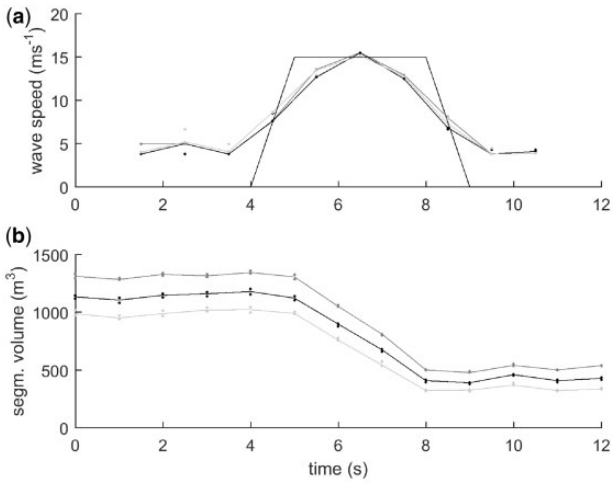

Figure 3. The estimated wave speed (a) and segmented volume (b). The speed used in the simulations of the turning wave is shown in the straight black lines (A). The effect of the decreased, base line and increased segmentation threshold (multiplied by $k = 0.8$, 1, and 1.2 is shown as dark grey, black and light grey lines, respectively, whereas the dots denotes increased or decreased level of smoothing for each segmentation threshold, respectively. Note the reduction of volume as the turning wave causes the segmented volume to decrease.

The edge tracking algorithm was applied to the data from the classification algorithm. The parameter M was set to 3, which caused the edges of the first time step to be tracked backwards and forward over the three following time steps. The gradual increase in the speed was caused by averaging over fourr-time steps ($M = 3$), and that is the reason for the discrepancy between the estimated and the real speed (Figure 3A). In addition, the volume of the segmentation for each time step was calculated (Figure 3B) to assess the reliability of the segmentation algorithm and to relate it to the wave estimates. As expected, the reduction in volume corresponded to the estimated behavioural wave speed. Furthermore, the sensitivity to the smoothing parameter was low for both the wave speed and the volume, which indicates consistent results for different levels of smoothing. The sensitivity to the shift in threshold was low for the wave speed, whereas the change did affect the segmented volume. This was expected since a reduction in threshold will cause the segmented volume to increase. However, the important property is how it changes, and trends in volume change remained consistent.

Testing on real data

The method was applied to two datasets of MS70 data observing herring, aboard RV "G.O. Sars" in the Norwegian Sea (Cases II and III). The schools were migrating to overwintering areas along the coast of Northern Norway, and were under high predation pressure from fishing vessels and whales. Killer whales (*Orcinus orca*) were observed attacking a different school some hours before Case III. Weather conditions were calm in both cases, resulting in low surface scattering. No irregular noise from whales or from other vessels was observed. Both cases included turning events (Figure 4), where Case II included a large and highly structured school whereas Case III was a more distinct school.

For Case II, the school was ∼300 m in diameter, located at 50 m depth, and was observed by passing the school for 3 min in a south-southeast direction several hours past sunset on 16 November 2009. The school was entering the sonar volume during data collection, causing partial coverage of the school and an increase in the total backscatter with time (Figure 4E). The variations in backscatter indicate a school that is in a highly dynamic state. The short observation period disallowed estimation of the direction of movement of the school.

In Case III the school was ∼100 m in diameter, located at 150 m depth, and was observed by circumnavigating the school for several rounds during one hour at an approximate distance of 300 m, just before sunrise on 17 November 2009. The school moved at an approximate speed of 1.0 m/s towards northeast, possibly affected by the sea current. The reduction in the total backscatter from incidence angle −90° (school observed from south) to 0° (school observed from east) (Figure 4F) indicates that the individuals were oriented east-west.

For both cases, 20-time steps were selected (UTC 15:38:37–15:39:08 for Case II and UTC 09:06:50–09:07:22 for Case III), and the data were processed in a similar manner to the simulated data, including coordinate transformation, smoothing and segmentation, followed by edge tracking (Supplementary Figures S2 and S3) and final speed estimation (Figure 5).

For Case II, when following the internal changes by viewing one depth slice (Supplementary Figure S2), there is an initial increase in segmented volume, indicating that the fish are increasingly orienting themselves perpendicular to the sonar beams and hence leading to an increase in total backscatter. This growth in area is consistent with a wave spreading outwards. However, from ping 9 and onwards, another part of the school appears that is not directly connected in space. Since this part is connected to the same segmentation volume at later time steps, this causes an overestimation of the velocities since the tracks jump across the open space. The segmented volume increases over the time series showing that there are substantial fluctuations, but the changes in volume cannot be clearly be attributed to the estimated turning wave speeds.

To evaluate the quality of the speed estimates, the sensitivity of the estimated wave speeds are used (Figure 5A). The wave speed estimates seem relatively stable over the parameters except for some large deviations between 10 and 20 s associated with the appearance of parts of the school, and some deviations also towards the end of the time series. Similar to Case I, the sensitivity of the estimated volume is directly dependent on the threshold, but shows the same trend for the three factors $k \in \{0.8,\ 1.0,\ 1.2\}$. Case II demonstrates that the wave estimation fails when segments are connected over larger distances via connected voxels in later time steps, but that the sensitivity metrics picks this up and can be used to flag the cases where the method fails. Furthermore, changes in the volume of the segmented voxels seem to be a reliable indicator of internal fluctuations in the school.

In Case III, the school is fully ensonified by the sonar (Figure 4C and D). There is a "vacuole" opening up in the sonar image progressing from the lower left corner towards the middle of the school (Figure 4D). When following one depth slice in the school (Supplementary Figure S3), there is a clear expansion followed by a reduction in the segmented volume. The increase and decrease is gradual, indicating a wave-like phenomenon. The wave speeds (Figure 5B) show two peaks of ∼10 m/s, and the sensitivity to the parameters are low indicating that the pattern is

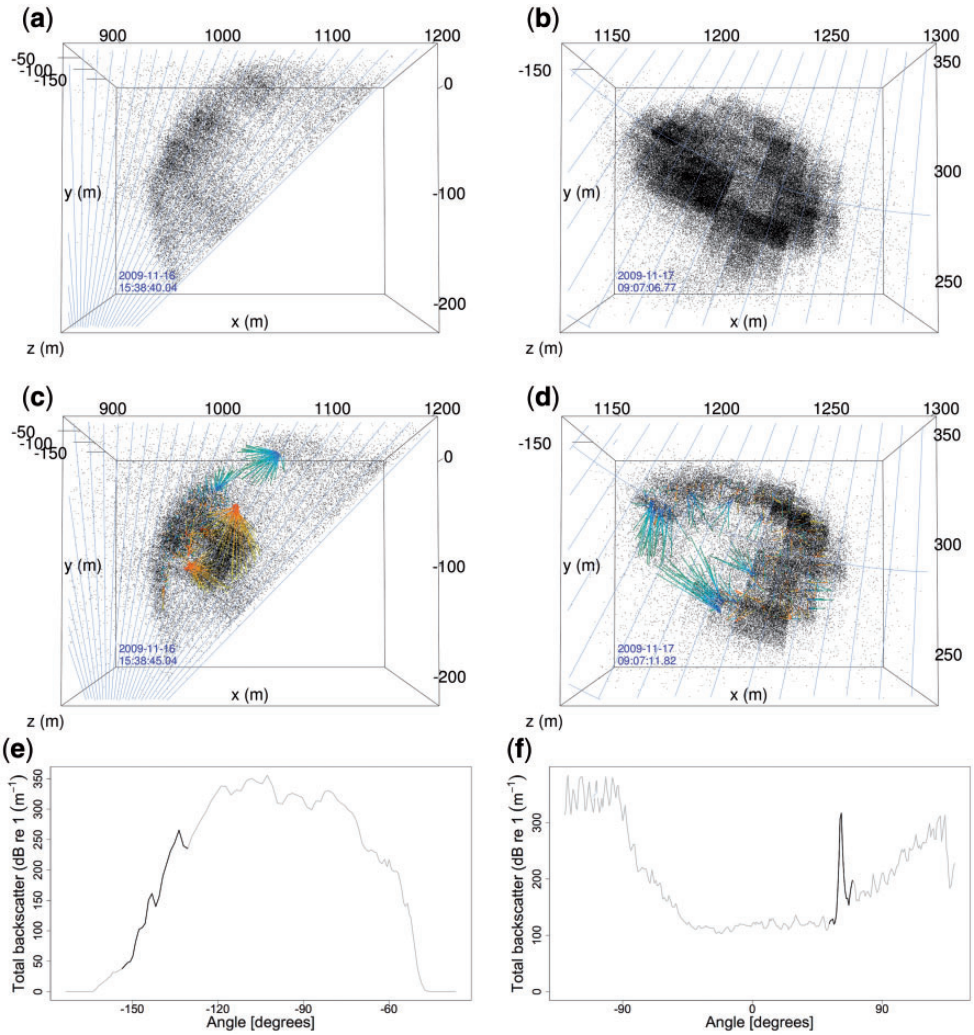

Figure 4. The real-data test-case examples II (left column) and III (right column), showing time step 3 (a) and 4 (c) for case II and 11 (b) and 14 (d) for case III, and the total backscatter for each case (e and f). (A–D) show 3D plots seen from above, where each black point represents a backscattering cross section of $3 \cdot 10^{-3}$ m^2, blue lines indicate the sonar beams, and the lines graded from yellow to orange and cyan to blue are the forward and backward tracks, respectively. The tracks are representative of the mean time of the plotted and the previous time step. (e and f) show the total backscatter of the school plotted versus incidence angle to the school, where at 0° and 90° the vessel is located east and north of the school, respectively. The 20 selected time steps are indicated in black for both cases.

robust to the choice of parameters. The peaks are associated with the expansion and reduction in segmented volume and are based on the forward and backward tracking, respectively. The segmented volume shows a peak after the initial expansion (Figure 5D), and the slope of the volume curve matches the velocity estimates well, i.e. high velocity corresponds to a steep increase or decrease in volume. Case III demonstrates that the wave estimation works well when there is a gradual increase in segmented volume, similar to the simulation case (Case I). It also shows that the sensitivity metrics work well as a quality indicator of the results.

Discussion

Our primary objective was to develop a methodology capable of extracting large scale behavioural waves in wild fish schools using 4D multi beam sonar. The method reliably estimated the waves when a clear expansion/reduction was seen, but was less effective when large and possibly independent fluctuations caused larger segmentation volumes to be lost or gained between time steps. In those circumstances, the sensitivity test can be used to flag the unsuccessful cases. Since the method was capable of resolving the waves in a more quantitative way compared with earlier studies, the objectives set out in the introduction were met.

A further evaluation of the method can be achieved by comparing the wave speeds with the estimates from previously published work. In tank observations of collective behavioural responses of schooling herring, the speed of information transfer has been measured to be 6.7 m/s (Marras *et al.*, 2012). These measurements were carried out in a tank of 10x6x1 m on 50 individual fish. In natural conditions, the speed of information transfer, or" waves of agitation", in schools of Peruvian anchovy (*Engraulis ringens*) exposed to predation was estimated to be 7.45 m/s (Gerlotto *et al.*, 2006). Another kind of "wave" is the forming speed of large-scale schools of herring at a speed of 3–3.5 m/s quantified using low-frequency acoustics (Makris *et al.*, 2009). The group movement in this case was typically 0.18 m/s, and the

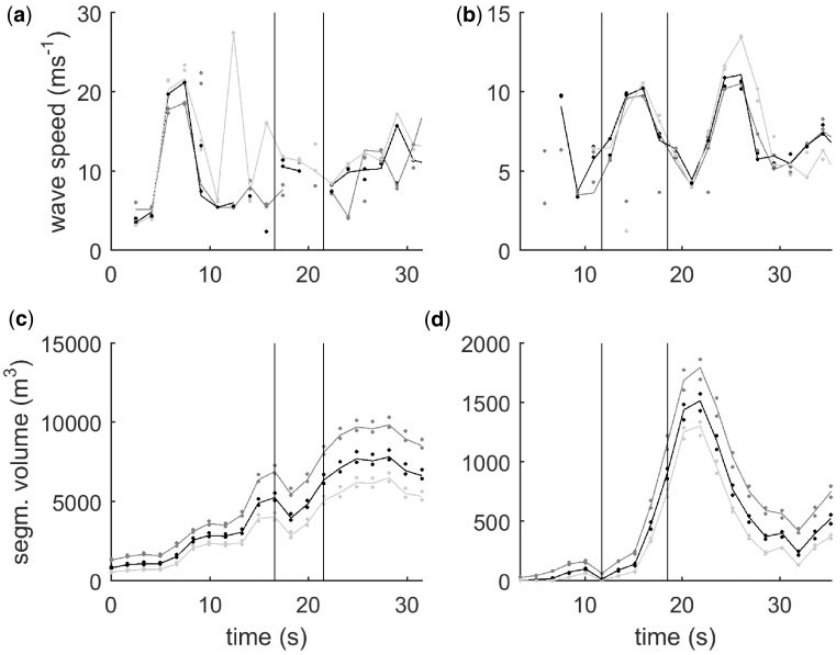

Figure 5. The estimated wave speeds (a,b) and segmented volumes (c,d) for Case II (A,C) and III (B,D). The effect of the decreased, base line and increased segmentation threshold (multiplied by $k = 0.8$, 1, and 1.2) is shown as dark grey, black, and light grey lines, respectively, whereas the dots denotes increased or decreased level of smoothing for each segmentation threshold, respectively. Note the difference in volume as the turning wave causes the segmented volume to change.

school forming speed was caused by the aggregation formation rather than behavioural changes like a wave of agitation. Our peak speed estimate was ∼10 m/s in the successful application (Case III), which is the same order of magnitude as these earlier studies. The wave speeds in the case studies fit the results from previously published work, but is capable of dealing with true 3D observations or larger spatial scales compared with earlier work.

Future expansion of the method could include tuning and optimization of the segmentation algorithm, particularly on how the segmentation method deals with overall changes in backscattering strength. This is not critical for short test cases as presented in this article, but should be a topic of attention for long duration data sets with substantial changes in overall backscatter throughout the data set. It is also worth noting that some ensonification angle-changes cause a stronger shift in the signal leading to clearer definition of the waves as opposed to other angles, and that there is a 180 ambiguity if large orientation changes occurs. In addition, the 60° horizontal and 45° vertical range of the observation volume of the sonar may result in variations in backscatter throughout a school even when all fish have a common mean orientation. Finally, the detectability of short distance waves will be reduced by range from the sonar, due to the decrease in resolution of the acoustic data across beams by increasing range. In addition, a low pulse repetition rate and high M may underestimate the speed of the waves. All these effects may bias the frequency of occurrence of the waves, but the wave speed estimates themselves should be robust. Noise in the data could potentially be detected as behavioural waves by the method, but then the noise must be spatially correlated and move through the sonar volume over several time steps, which is not likely. The noise can, however, mask the wave speed estimates if the difference in backscatter between the school and the noise is low, resulting in fluctuations in the boundary of the segmentations.

As opposed to earlier methods, our method works on three spatial dimensions and enables investigation into the vertical structure of the school. Earlier more manual methods have been restricted to two spatial dimensions and time (Gerlotto *et al.*, 2006; Handegard *et al.*, 2012). Our method allows for testing of whether waves progress in the vertical dimension as well as the horizontal (Figure 4, Supplementary Video). We have estimated a single maximum wave speed for the school to illustrate the method, but the method supports development of a more comprehensive 3D analysis of the data.

In particular, application of the method can serve to quantify group responsiveness of wild fish schools exposed to various external factors such as predators, environmental perturbations or anthropogenic disturbances. The method can be used to scale up and validate controlled experiments on noise playbacks (Handegard *et al.*, 2014, 2016), predator awareness (Rieucau *et al.*, 2016a, b), density dependent escape responses (Rieucau *et al.*, 2014), and would help ascertain the proximate mechanisms that underlie the transfer of information in massive schools (Rosenthal *et al.*, 2015). Applying the method on simulated data based on state-of-the-art IBMs, and comparing the results to those of wild fish schools, can be used to evaluate the ability of the IBMs to predict the collective maneuvers of real schools. These applications of the method would ultimately shed light on the selective pressures that have shaped the formation, maintenance and reactions of massive schools in marine fish.

Our method could also have applied ramifications. Understanding the variability in side-aspect backscattering processes (Pedersen *et al.*, 2009) can be used to improve

understanding of biases in fisheries independent acoustic surveys (Løland *et al.*, 2007), especially biases related to fish distribution and behaviour (De Robertis and Handegard, 2013) using horizontally looking sonars.

Methods to observe the collective behavioural mechanisms *in situ* are particularly important. Until now, existing methodology was restricted to small scale laboratory experiments or qualitative observations, and although the level of detail is less our approach provides a method to validate the generalizations that are usually extrapolated from small scale tank studies. The proposed method can do this, and is thus an important building block when applying the knowledge of the structure, dynamics and function of fish schools acquired from small scale experiments to natural environments.

Supplementary data

Supplementary material is available at the *ICESJMS* online version of the article.

Acknowledgements

We are grateful to Gavin Macaulay for constructive comments and language editing help during the writing process.

Funding

This work was financed by the Norwegian Research Council (grant 204229/F20).

References

Axelsen, B. E., Anker-Nilssen, T., Fossum, P., Kvamme, C., and Nøttestad, L. 2001. Pretty patterns but a simple strategy: predator-prey interactions between juvenile herring and Atlantic puffins observed with multibeam sonar. Canadian Journal of Zoology-Revue Canadienne De Zoologie, 79: 1586–1596.

Ballerini, M., Cabibbo, N., Candelier, R., Cavagna, A., Cisbani, E., Giardina, I., Lecomte, V. *et al.* 2008. Interaction ruling animal collective behavior depends on topological rather than metric distance: evidence from a field study. Proceedings of the National Academy of Sciences of the United States of America, 105: 1232–1237.

Benoit-Bird, K. J., and Lawson, G. L. 2016. Ecological insights from pelagic habitats acquired using active acoustic techniques. Annual Review of Marine Science, 8: 463–490.

Berdahl, A., Torney, C. J., Ioannou, C. C., Faria, J. J., and Couzin, I. D. 2013. Emergent sensing of complex environments by mobile animal groups. Science, 339: 574–576.

Bertsatos, I., and Makris, N. C. 2011. Estimating the instantaneous velocity of randomly moving target swarms in a stratified ocean waveguide by Doppler analysis. The Journal of the Acoustical Society of America, 130: 84–101.

Buhl, J., Sumpter, D. J. T., Couzin, I. D., Hale, J. J., Despland, E., Miller, E. R., and Simpson, S. J. 2006. From disorder to order in marching locusts. Science, 312: 1402–1406.

Cavagna, A., Cimarelli, A., Giardina, I., Parisi, G., Santagati, R., Stefanini, F., and Viale, M. 2010. Scale-free correlations in starling flocks. Proceedings of the National Academy of Sciences of the United States of America. http://www.pnas.org/content/early/2010/06/11/1005766107 (last accessed 3 September 2012).

Couzin, I. D., Krause, J., Franks, N. R., and Levin, S. A. 2005. Effective leadership and decision making in animal groups on the move. Nature, 433: 513–516.

De Robertis, A., and Handegard, N. O. 2013. Fish avoidance of research vessels and the efficacy of noise-reduced vessels: a review. ICES Journal of Marine Science, 70: 34–45.

Fréon, P., Gerlotto, F., and Soria, M. 1992. Changes in school structure according to external stimuli: description and influence on acoustic assessment. Fisheries Research, 15: 45–66.

Garcia, D. 2010. Robust smoothing of gridded data in one and higher dimensions with missing values. Computational Statistics and Data Analysis, 54: 1167–1178.

Gerlotto, F., Bertrand, S., Bez, N., and Gutierrez, M. 2006. Waves of agitation inside anchovy schools observed with multibeam sonar: a way to transmit information in response to predation. ICES Journal of Marine Science, 63: 1405–1417.

Handegard, N. O., Boswell, K., De Robertis, A., Macaulay, G. J., Rieucau, G., and Sivle, L. D. 2016. Investigating the effect of tones and frequency sweeps on the collective behavior of penned herring (Clupea harengus). Advances in Experimental Medicine and Biology, 875: 391–398.

Handegard, N. O., Boswell, K. M., Ioannou, C. C., Leblanc, S. P., Tjøstheim, D. B., and Couzin, I. D. 2012. The dynamics of coordinated group hunting and collective information transfer among schooling prey. Current Biology, 22: 1213–1217.

Handegard, N. O., Robertis, A. D., Rieucau, G., Boswell, K., and Macaulay, G. J. 2014. The reaction of a captive herring school to playbacks of a noise-reduced and a conventional research vessel. Canadian Journal of Fisheries and Aquatic Sciences, 72: 491–499.

Hemelrijk, C. K., Reid, D. A. P., Hildenbrandt, H., and Padding, J. T. 2015. The Increased Efficiency of Fish Swimming in a School. Fish and Fisheries, 16: 511–521.

Herbert-Read, J. E., Perna, A., Mann, R. P., Schaerf, T. M., Sumpter, D. J. T., and Ward, A.J.W. 2011. Inferring the rules of interaction of shoaling fish. Proceedings of the National Academy of Sciences of the United States of America, 108: 18726–18731.

Hofmann, H. A., Beery, A. K., Blumstein, D. T., Couzin, I. D., Earley, R. L., Hayes, L. D., Hurd, P. L. *et al.* 2014. An evolutionary framework for studying mechanisms of social behavior: NESCent Working Group on Integrative Models of Vertebrate Sociality: Evolution, Mechanisms, and Emergent Properties. Trends in Ecology and Evolution, 29: 581–589.

Holmin, A. J., Handegard, N. O., Korneliussen, R. J., and Tjostheim, D. 2012. Simulations of multi-beam sonar echos from schooling individual fish in a quiet environment. The Journal of the Acoustical Society of America, 132: 3720–3734.

Holmin, A. J., Korneliussen, R. J., and Tjøstheim, D. 2016. Estimation and simulation of multi-beam sonar noise. The Journal of the Acoustical Society of America, 139: 851–862.

Huth, A., and Wissel, C. 1992. The Simulation of the Movement of Fish Schools. Journal of Theoretical Biology, 156: 365–385.

Jagannathan, S., Horn, B. K. P., Ratilal, P., and Makris, N. C. 2010. Force estimation and prediction from time-varying density images. IEEE Transactions on Pattern Analysis and Machine Intelligence, 40: 1–18.

Katz, Y., Tunstrom, K., Ioannou, C. C., Huepe, C., and Couzin, I. D. 2011. Inferring the structure and dynamics of interactions in schooling fish. Proceedings of the National Academy of Sciences of the United States of America, 108: 18720–18725.

Lilja, J., Marjomäki, T. J., Jurvelius, J., Rossi, T., and Heikkola, E. 2004. Simulation and experimental measurement of side-aspect target strength of Atlantic salmon (Salmo salar) at high frequency. Canadian Journal of Fisheries and Aquatic Sciences, 61: 2227–2236.

Løland, A., Aldrin, M., Ona, E., Hjellvik, V., and Holst, J. C. 2007. Estimating and decomposing total uncertainty for survey-based abundance estimates of Norwegian spring-spawning herring. ICES Journal of Marine Science, 64: 1302–1312.

Lopez, U., Gautrais, J., Couzin, I. D., and Theraulaz, G. 2012. From behavioural analyses to models of collective motion in fish schools. Interface Focus, 2: 693–707.

Maclennan, D. N., Fernandes, P. G., and Dalen, J. 2002. A consistent approach to definitions and symbols in fisheries acoustics. ICES Journal of Marine Science, 59: 365–369.

Makris, N. C., Ratilal, P., Jagannathan, S., Gong, Z., Andrews, M., Bertsatos, I., Godø, O. R. *et al.* 2009. Critical population density triggers rapid formation of vast oceanic fish shoals. Science, 323: 1734–1737.

Marras, S., Batty, R. S., and Domenici, P. 2012. Information transfer and antipredator maneuvers in schooling herring. Adaptive Behavior, 20: 44–56.

Misund, O. A. 1993. Dynamics of moving masses: variability in packing density, shape, and size among herring, sprat, and saithe schools. ICES Journal of Marine Science, 50: 145–160.

Nagy, M., Akos, Z., Biro, D., and Vicsek, T. 2010. Hierarchical group dynamics in pigeon flocks. Nature, 464: 890–894.

Ona, E., Mazauric, V., Andersen, L. N. 2009. Calibration methods for two scientific multibeam systems. ICES Journal of Marine Science, 66: 1326–1334.

Otsu, N. 1979. A threshold selection method from gray-level histograms. IEEE Transactions on Systems, Man, and Cybernetics, 9: 62–66.

Parr, A. E. 1927. A contribution to the theoretical analysis of the schooling behaviour of fishes. Occasional Papers of the Bingham Collection, 1: 1–32.

Parrish, J., Viscido, S. V., and Grünbaum, D. 2002. Self-organized fish schools: an examination of emergent properties. The Biological Bulletin, 202: 296–305.

Pedersen, G., Handegard, N. O., and Ona, E. 2009. Lateral-aspect target-strength measurements of in situ herring (Clupea harengus). ICES Journal of Marine Science, 66: 1191–1196.

Pitcher, T. J., Misund, O. A., Fernö, A., Totland, B., and Melle, V. 1996. Adaptive behaviour of herring schools in the Norwegian Sea as revealed by high-resolution sonar. ICES Journal of Marine Science, 53: 449–452.

Radakov, D. 1973. Schooling in the Ecology of Fish. John Wiley and Sons, New York.

Reynolds, C. W. 1987. Flocks, herds, and schools: a distributed behavioural model. Computer Graphics, 21: 25–34.

Rieucau, G., Boswell, K. M., Kimball, M. E., Diaz, G., and Allen, D. M. 2015. Tidal and diel variations in abundance and schooling behavior of estuarine fish within an intertidal salt marsh pool. Hydrobiologia, 753: 149–162.

Rieucau, G., De Robertis, A., Boswell, K. M., and Handegard, N. O. 2014. School density affects the strength of collective avoidance responses in wild-caught Atlantic herring Clupea harengus: a simulated predator encounter experiment. Journal of Fish Biology, 85: 1650–1664.

Rieucau, G., Holmin, A. J., Castillo, J. C., Couzin, I. D., and Handegard, N. O. 2016a. School level structural and dynamic adjustments to risk promote information transfer and collective evasion in herring. Animal Behaviour, 117: 69–78.

Rieucau, G., Sivle, L. D., and Handegard, N. O. 2016b. Herring perform stronger collective evasive reactions when previously exposed to killer whales calls. Behavioral Ecology, 27: 538–44.

Rosenthal, S. B., Twomey, C. R., Hartnett, A. T., Wu, H. S., and Couzin, I. D. 2015. Revealing the hidden networks of interaction in mobile animal groups allows prediction of complex behavioral contagion. Proceedings of the National Academy of Sciences of the United States of America, 112: 4690–4695.

Sund, O. 1935. Echo sounding in fishery research. Nature, 135: 953.

Tang, Y., Nishimori, Y., and Furusawa, M. 2009. The average three-dimensional target strength of fish by spheroid model for sonar surveys. ICES Journal of Marine Science, 66: 1176–1183.

Treherne, J. E., and Foster, W. A. 1981. Group transmission of predator avoidance behaviour in a marine insect: the trafalgar effect. Animal Behaviour, 29: 911–917.

Vabø, R., and Nøttestad, L. 1997. An individual based model of fish school reactions: predicting antipredator behaviour as observed in nature. Fisheries Oceanography, 6: 155–171.

Zhao, X., and Ona, E. 2003. Estimation and compensation models for the shadowing effect in dense fish aggregations. ICES Journal of Marine Science, 60: 155–163.

Handling editor: David Demer